Adsorption 11: 245–257, 2005


# Self-Diffusion Coefficients for Pure and Mixed Adsorbate Fluids in Narrow Pores

YURIY K. TOVBIN
*Karpov Research Institute of Physical Chemistry, ul. Vorontsovo pole 10, Moscow, 103064 Russia*
*tovbin@cc.nifhi.ac.ru*

**Abstract.** The equilibrium distribution and the concentration dependence of the local and average self-diffusion coefficients for pure fluid and binary mixture components in narrow slitlike pores were analyzed. The coefficients were calculated using the lattice gas model in the quasi-chemical approximation on the assumption of a spherical shape and approximately equal sizes of the components. For the pure adsorbate, these calculations were compared with molecular dynamics simulations. Both methods gave similar concentration profile changes and dynamic characteristics of interlayer particle redistributions in strong nonuniform adsorption fields for dense fluids. A satisfactory agreement was obtained for the temperature dependences of the self-diffusion coefficients along the pore axis. The influence of the molecule–wall potential and of intermolecular interaction were considered. The self-diffusion coefficients of the adsorbate were shown to strongly depend on the density of the mixture and the distance from pore walls.

**Keywords:** isotherms, coefficient of self-diffusion, argon, krypton, mixture, carbon slitlike pore

## 1. Introduction

Transport of molecules in porous media determines the characteristics of diverse catalytic, adsorption, and membrane processes (Timofeev, 1962; Kheifets and Neimark, 1982; Satterfield, 1970; Ruthven, 1984; Dubinin and Serpinskii, 1983; Mason and Malinauskas, 1983). The potential of walls in narrow pores (that is, pores up to 10 nm wide (Tovbin et al, 1993, 2001a)) influences the state of aggregation of fluids and, accordingly, the mechanisms of their transport. The most important dynamic characteristic is the self-diffusion coefficient. Its theoretical calculations over wide ranges of pore fillings (in the gaseous and liquid states) and temperatures is a difficult problem. Therefore currently, the self-diffusion coefficients of adsorbates are largely determined by the method of molecular dynamics (Todd, 1995; MacElroy, 1994; Akhmatskaya et al., 1997). Also recall that the available experimental methods for measuring self-diffusion coefficients (NMR and tracer techniques) give values that strongly differ from the data obtained from flow characteristics (Dubinin and Serpinskii, 1983; Vartapetyan et al., 1997), although some positive examples were appeared also (Karger, 2003). The situation with mixtures is still more complex. In particular, the question of the concentration dependences of these coefficients for dense gases and liquids in narrow pores remains open in many respects.

In recent years, the lattice gas model (LGM) (Tovbin, 1991; Hill, 1956) has allowed considerable progress to be made in describing the transfer of molecules in narrow pores. This model has been used to analyze the phase diagrams of adsorbates comprising spherical molecules in slitlike and cylindrical pores (Tovbin et al, 1998b, 1999c, 2001b) and to obtain the first results in studies of the dynamic characteristics (self-diffusion, shear viscosity, and heat conductivity coefficients) of adsorbates in narrow pores (Tovbin, 2001a, 2002a, 2002c). The LGM agrees very closely with phase diagrams (Votyakov et al., 1999, 2000) and satisfactorily agrees with calculations of self-diffusion coefficients in cylindrical pores and shear viscosity coefficients in slitlike pores (Tovbin, 2002a; Tovbin et al., 2003a).

In this work, using the LGM (Tovbin, 1991) we suggest to study the concentration dependence of the self-diffusion coefficients for pure fluid and binary mixture components over a wide range of narrow pore fillings, from dense gases to liquids. This approach requires much less computational time and provides close agreement with molecular dynamics calculations of the self-diffusion coefficients of one-component fluids. However, comparisons such as these are of an episodic nature, and the applicability of lattice gas model to the description of the dynamic characteristics of adsorbates in porous systems and the accuracy of such descriptions have not been conclusively clarified. This problem is extraordinarily relevant because of large time expenditures involved in molecular dynamics calculations, which are up to $10^5$ times larger than for similar calculations using the lattice gas model. In addition, despite studies by numerical methods (Gelb et al., 1999), it was the lattice gas model that allowed the multi-domes character of phase diagrams in narrow-pore systems to be revealed and explained (Tovbin et al., 2002). At the same time, the lattice model involves approximate calculations based on the quasichemical approximation; this requires controlling the accuracy of the results, especially those obtained near critical regions (which is why the principle of jointly using the quasi-chemical approximation and exact methods was first drawn up (Tovbin, 2003b)).

Our main goal was to pass to a self-consistent description of the equilibrium and dynamic characteristics of the adsorption of mixture components in narrow pores by analogy with one-component fluids discussed in the papers (Tovbin, 2002a; Votyakov et al., 1999, 2000; Tovbin et al., 2003a). We restrict our consideration to components with spherical shapes and approximately equal sizes. Strictly, this makes our results only applicable to isotopic mixtures, because all molecules have different sizes. This approximation, however, allows correct results to be obtained for many mixtures of molecules whose sizes differ not too strongly and is therefore extensively used in studying volume solutions (Prigogine, 1957; Smirnova, 1987). The lattice gas model itself can be applied to mixtures of molecules of different sizes (Prigogine, 1957; Smirnova, 1987; Tovbin, 1997b, 1998a, 1999; Tovbin et al., 2001). In addition, we only consider monodisperse porous systems (the equations for the adsorption isotherms of a mixture of spherical molecules of approximately equal sizes in a polydisperse system of slitlike pores were obtained in the paper (Tovbin, 2004).

In this work, we compare distribution profiles and the characteristics of adsorbate mobility in slitlike pores in a wide temperature range for various fluid-wall interaction energies. The resultant flow of thermal motion of molecules in a certain direction in a nonuniform system, such as a fluid in adsorption potential fields of pore walls, can be expressed through local self-diffusion coefficients and the average self-diffusion coefficient over the pore cross section (Tovbin, 1991, 1990a, 1990b). In order to calculate self-diffusion coefficients, we must first obtain the equilibrium local distributions of mixture components over the section of a pore. The character of the distribution of mixture components strongly depends on the type of the adsorbent–adsorbate potential and the width of the pore. The mean component distributions over pore sections determine the partial adsorption isotherms at fixed external pressures of mixture components.

## 2. The Lattice-Gas Model

### *2.1. The Model and Local Isotherms*

In the lattice gas model (Tovbin, 1991, 1996) the volume $V_p$ of a slitlike pore is divided into monoatomic layers arranged parallel to the pore walls. Each layer is divided into cells that are equal to the volume of a particle $v_0 = \lambda^3$ to exclude doubly filling a cell (adsorption center or site) by different molecules. We then have $V_p = Nv_0$, where $N$ is the number of cells in the system. Let us denote the number of the nearest sites in the lattice structure by $z$. Only one particle can be situated in each site, either a molecule of kind $i$ (if the center of mass of the molecule is inside the cell) or vacancy $v$. Index $i$ numbers mixture components. Let $s$ denote the number of different occupancy states of a site in the system; that is, the number of components is $s - 1$.

The concentration of molecules is usually assumed to equal the number of these molecules $N_i$ in the unit volume, $c_i = N_i / V_p$. In the LGM, the concentration of a fluid component is characterized by the $\theta_i = N_i /N$ value, which is the ratio between the actual number of particles in some volume and the maximum possible number of the same particles closely packed in the same volume. We then have $\theta_i = c_i\, v_0$. The local density of particles $i$ in cell $f$ will be denoted by $\theta_f^i$. Obviously,

$$\sum_{i=1}^{s-1} \theta_f^i + \theta_f^s = 1\cdot \qquad (1)$$

The average partial fluid concentration $\theta_i$ and the total average pore filling $\theta$ can be written in terms of local concentrations as

$$\theta_i(\{P\}) = \sum_{f=1}^{t} F_f\, \theta_f^i(\{P\}), \quad \theta(\{P\}) = \sum_{i=1}^{s-1} \theta_i(\{P\}), \tag{2}$$

where $F_f$ is the fraction of sites of type $f$. The $\{P\} \equiv P_1, \ldots, P_{s-1}$ symbol is used to denote the set of all partial pressures of mixture components $P_i$, $1 \le i \le s-1$. Every cell $f$ is characterized by its own interaction energy $Q_f^i$ between molecules of kind $i$ and pore walls and, accordingly, its own Henry constant $a_f^i$. All lattice sites can be divided into groups with equal properties according to this parameter. The number of such groups will be denoted by $t$. If the pore walls are homogeneous, all sites in one layer are equivalent. The number $f$ of a layer therefore coincides with the number of the site it contains. If the number of monolayers is even, $t = H/2$, and if it is odd, $t = (H+1)/2$ ($H$ is the width of the pore). The local Henry constant is $a_f^i = a_f^{i0} \exp(\beta Q_f{}^i)$, where $\beta = (kT)^{-1}$ and $a_f{}^{i0} = \beta F_i/F_i{}^0$, here $a_f{}^{i0}$ is the preexponential factor of the Henry constant; $F_i$ and $F_i^0$ are the partition functions of molecules $i$ in the lattice system and outside it (in the gas phase), respectively; $Q_f^i$ is the interaction energy between molecule $i$ in layer $f$ and pore walls calculated as $= u_i(f) + u_i(H-f+1)$, $1 \le f \le t$ (here, the interaction potential between a molecule and a pore wall $u_i(f) = \varepsilon_i / f^3$ corresponds to the attractive branch of the (3–9) Mie potential (Steele, 1974); and $\varepsilon_i$ is the energy parameter of the potential. Accordingly, the fraction of sites $F_f$ in layer $f$ is $2/H$ for even $H$; for odd $H$, it is $2/H$ if $1 \le f \le (t-1)$ and $1/H$ if $f = t$. The normalization condition for sites of various types has the form

$$\sum_{f=1}^{t} F_f = 1 \tag{3}$$

The local partial adsorption isotherms $\theta_f{}^i(\{\mathrm{P}\})$ of various adsorption centers, which are needed for Eqs. (2), are calculated by the system of equations from the papers (Tovbin, 1991, 1996). These equations take into account energetic nonuniformity of lattice sites and intermolecular interactions at a distance of $R$ coordination spheres,

$$a_f^i\, P_i = \theta_f^i\, \Lambda_f^i \,/\, \theta_f^v, \tag{4}$$

$$\Lambda_f^i = \prod_r \prod_g \left(1 + \sum_{j=1}^{s-1} x_{fg}^{ij}(r)\, t_{fg}^{ij}(r)\right)^{z_{fg}(r)},$$

$$x_{fg}^{ij}(r) = \exp(-\beta \varepsilon_{fg}^{ij}(r)) - 1,$$

where the $\Lambda_f^i$ function describes nonideality of the adsorption system in the quasi-chemical approximation.

Equation (4) describes of layered distributions of sites of various types in slitlike pores: $z_{fg}(r)$ is the number of neighboring sites in layer $g$ at distance $r$ from the site under consideration in layer $f$. It indicates that the lateral interaction parameter $\varepsilon_{fg}^{ij}$(r) between neighboring molecules $i$ and $j$ separated by $r$ coordination spheres may be a function of temperature and local composition around sites $f$ and $g$, whereas interactions of all molecules ($i = s-1$) with vacancies ($j = s$) as well as between vacancies ($i, j = s$) are zero. Index $g$ runs over all neighbors $z_f(r)$ of site $f$ at distance $r \le R$ within the pore, where $R$ is the radius of the interaction potential.

The $t_{fg}^{ij}(r) = \theta_{fg}^{ij}(r)/\,\theta_f^i$ functions describe the conditional probabilities of the presence of a neighboring particle $j$ in a site of type $g$ at distance $r$ from the central particle $i$ in a site of type $f$, whereas the $\theta_{fg}^{ij}(r)$ functions describe similar full probabilities. These last functions satisfy the equations

$$\theta_{fg}^{ij}(r) = \theta_{fg}^{ss}(r) = \theta_{fg}^{is}(r)\theta_{fg}^{sj}(r) \exp[\beta \varepsilon_{fg}^{ij}(r)], \tag{5}$$

which are solved using the normalization conditions

$$\sum_{j=1}^{s} \theta_{fg}^{ij}(r) = \theta_f^i, \quad \sum_{i=1}^{s} \theta_{fg}^{ij}(r) = \theta_g^j, \tag{6}$$

together with the Eq. (1).

The equilibrium distribution of particles over sites of various types was found from system (1)–(6) by the Newton iterative method for selected $\{\theta_i\}$ or $\{P_i\}$ sets. The mean root square at solving (1)–(6) was less than 0.1%.

### 2.2. *The Thermal Velocity of the Motion of Molecules*

The large difference in the local densities across a pore when molecules are strongly attracted to pore walls requires a self-consistent description of the motion of molecules both in the rarefied vapor regions in the pore center and in dense liquid regions near pore walls. Under these conditions, the free-path concept is difficult

to use, because free paths in the liquid and vapor phases can differ by four orders of magnitude. Instead of the free path, the lattice model uses the probability of a jump of a molecule of kind $i$ ($W_i(\rho)$) through distance $\rho$:

$$W_i(\rho) = U^i_{fg}(\rho)/\theta_f, \tag{7}$$

where $U_{fg}{}^i(\rho)$ is the average velocity (or average frequency) of jumps of molecules $i$ from cell $f$ to free cell $g$ through distance $\rho$. The velocity of particle jumps is calculated using the Eyring transition state model (Glasstone et al., 1941), which treats displacements of molecules as an activation process of overcoming the barrier. The formulation of this model for nonideal reaction systems, when the barrier to be overcome is created by the potential of neighboring particles and the surface of a solid, is given in the papers (Tovbin, 1991, 1990a, 1990b, 1984). At equilibrium, we have

$$U^i_{fg}(\rho) = K^{iv}_{fg}(\rho)V^{iv}_{fg}(\rho),\ V^{iv}_{fg}(\rho) = \theta^{iv}_{fg}(\rho)\Lambda^i_{fg}(\rho), \tag{8}$$

$$\theta^{iv}_{fg}(\rho) = \theta^{iv}_{fg(1)}(1)\prod_{\xi} t^{vv}_{\xi\xi+1}(1),$$

$$K^{iv}_{fg}(\rho) = (8/\pi m_i\beta)^{1/2}\exp[-\beta E^{iv}_{fg}(\rho)]/4\rho,$$

where $K^{iv}_{fg}(\rho)$ is the rate constant for jumps of molecule $i$ from cell $f$ to free cell $g$ through distance $\rho$ on an unfilled lattice; $E^{iv}_{fg}(\rho)$ is the activation energy of jumps through distance $\rho$ near the walls where their adsorption potential is noticeable, $E^{iv}_{fg}(\rho)$ is nonzero (for cells far from the pore walls, $E^{iv}_{fg}(\rho) = 0$); $m_i$ is the mass of molecule $i$; and $h$ is the Planck constant.

The concentration dependence of the velocity of molecule migration is described by the multiplier $V^{iv}_{fg}(\rho)$. It takes into account two factors: (1) the probability of the existence of a free trajectory of length $\rho$ from cell $f$ to cell $g$ (a trajectory not blocked by other molecules) and (2) the influence of lateral interactions with neighboring molecules that surround the given trajectory on the probability of a jump along it; these interactions are described by the function of nonideality of the system $\Lambda^i_{fg}(\rho)$. The $\theta^{iv}_{fg}(\rho)$ function is constructed in terms of the probabilities of the existence of a sequence of free cells $g(1)$, $g(2)$, and so on up to cell $g = g(\rho)$ that form the given trajectory. The number of multipliers in the product over $\xi$ in (8) is $(\rho - 1)$. (For $\rho = 1$, $g(1)$ is the end cell.) The $\Lambda^i_{fg}(\rho)$ function is written as (Tovbin, 1991, 1990a, 1990b, 1984)

$$\Lambda^{iv}_{fg}(\rho) = \prod_{r=1}^{R}\prod_{\omega_r=1}^{\pi_r}\prod_{h\in m(\omega_r)} \times\sum_{j=1}^{v}\frac{\theta^{ij}_{fh}(r_1)\,\theta^{vj}_{gh}(r_2)}{\theta^i_f\,\theta^v_g\,\theta^j_h}\Bigg) E^{ivj}_{fgh}(\omega_r), \tag{9}$$

$$E^{ivj}_{fgh}(\omega_r) = exp\{\beta[\delta\varepsilon^{ij}_{fh}(r_1) + \delta\varepsilon^{vj}_{gh}(r_2)]\},$$

$$\delta\varepsilon^{ij}_{fh}(r) = \varepsilon^{*ij}_{fh}(r) - \varepsilon^{ij}_{fh}(r),$$

where $\varepsilon^{*ij}_{fh}(r)$ is the interaction parameter between the activated complex of the molecule $i$ migrating from site $f$ to free site $g$ through distance $r$ and a neighboring molecule in the ground state in site $h$, $r \le R$. (We used the dimensionless parameter $\alpha = \varepsilon^*/\varepsilon$ in the calculations.) The distance between sites $h$ and $f$ is $r_1$, and the distance between $h$ and $g$ is $r_2$. The symbol $\omega_r$ characterizes the position of site $h$ in terms of the angle between two lines (the first line connecting the pair of "central" sites $f$ and $g$, whereas the second line connecting site $h$ with the middle of the $fg$ line) and the distance $r$ from one of the two central sites $f$ and $g$; $m(\omega_r)$ is the set of neighboring sites with fixed $r$ and $\omega_r$ values.

In the absence of lateral interactions, (8), (9) is written as $U^i_{fg}(\rho) = K^{iv}_{fg}\theta_f(1 - \theta_g)^\rho$.

So, the average thermal velocity of the motion of molecules is defined as

$$w^i_{fg} = \rho W_i(\rho) = \rho U^i_{fg}(\rho)/\theta^i_f \tag{10}$$

Far from the pore walls at low density ($\theta \to 0$), we have $w^i_{fg} = (8/\pi m_i\beta)^{1/2}$, which equals the mean thermal velocity of molecules in the gas phase (Hirschfelder et al., 1954).

### 2.3. *Self-Diffusion Coefficients*

Self-diffusion coefficients characterize the motion of a labelled molecule under the conditions of equilibrium distribution of all the components in the space under consideration. In practice, they are usually correlated with the motion of a tracer introduced into some local region of the system, and the time dependence of its redistribution over the remaining part of the solution is measured. In the presence of external fields (in our problem, the field of the surface potential of

pore walls) in a heterogeneous system, we distinguish between local and average self-diffusion coefficients (Tovbin, 1990a).

The local self-diffusion coefficient characterizes the redistribution of molecules $i$, $1 \le i \le s-1$, between neighboring sites $f$ and $g$ in neighboring planes at distance $\rho$ from each other,

$$D_{fg}^{*i}(\rho) = z_{fg}^{*}\rho^2\, U_{fg}^{i}(\rho)/\theta_f^i, \tag{11}$$

where $z_{fg}^{*}$ is the number of possible jumps between neighboring sites for each cell $f$ and $U_{fg}^{i}(\rho)$ is given by Eqs. (8) and (9). The structure of this equation shows that the self-diffusion coefficients of all components substantially depend on the local distributions of the components across the pore and the direction of the motion under consideration.

The average self-diffusion coefficient is determined over the region containing a variety of local regions. The motion of labelled molecules along the axis of the pore is characterized by the equation obtained through averaging over all sites in its cross section. The average self-diffusion coefficient of component $i$ $(1 \le i \le s-1)$ in a slitlike pore is described by the equation

$$\mathrm{D}_{\mathrm{i}}^{*} = \sum_{\rho} \rho^2 \sum_{q=1}^{t} F_q \sum_{p=1}^{t} z_{qp}(\rho) \frac{U_{qp}^{i}(\rho) d\,\theta_q^{*i}}{\theta_q^i\, d\theta_i^{*}} \tag{12}$$

where $z_{qp}$ is the number of bonds between a site in layer $q$ and neighboring sites in layer $p$ and $\mathrm{d}\theta_q^{*i}/\mathrm{d}\theta_i^{*} = \mathrm{d}\theta_q^i/\mathrm{d}\theta_i$. The jump constants and local Henry constants are related as $a_q^i\, K_{qp}^{iv} = a_p^i\, K_{pq}^{iv}$.

## 3. Equilibrium and Dynamic Properties of Pure Fluid and Binary Mixture in Narrow Slitlike Pores

We performed calculations on the assumption that slitlike pore walls consisted of various materials: graphite atoms, $SiO_2$ groups or some polymer material with small adsorbent—adsorbate energy $Q_1^1$. This upper index $i = 1$ corresponds to argon atoms, which was the pure fluid or one of the mixture components. For argon and carbon walls, parameters were set constant $Q_1^1 = 9.24\ \varepsilon_{ArAr}$ at $\varepsilon_{ArAr}/k_B = 119$ K, whereas the properties of the second component were varied; for krypton atoms $Q_1{}^2 = 12.17\ \varepsilon_{ArAr}$ (Steele, 1974; Sokolowski et al., 1990). Lateral interactions $\varepsilon$ were determined by the Lennard-Jones potential $U_{ij} = 4\varepsilon_{ij}[(\sigma_{ij}/r)^{12} - (\sigma_{ij}/r)^6]$, $i, j = 1$ and 2, with $r/\sigma_{ij} = 1.12$, which corresponds to the potential minimum. The interaction parameter between particles of different kinds was estimated as $\varepsilon_{12} = (\varepsilon_{11}\varepsilon_{22})^{1/2}$.

The width of the pore was varied from 3 to 25 monolayers. It was assumed that the radius of the adsorbate–adsorbent interaction potential equaled three. This gave equivalent layer fillings starting with the fourth monolayer. Our calculations were restricted by using the nearest jumps with $\rho = 1$ (it is obvious meaning for dense fluids; for rarefied fluids it gives qualitative correct results).

### 3.1. *Analysis of the Local Mobility of Particles*

A special procedure for processing molecular dynamics (MD) trajectories was developed for comparing the LGM and MD results (Mazo et al., 2003). Characteristics about molecule mobilities during their interlayer redistribution and the average self-diffusion coefficients along the pore axis were considered. As the "layer" distribution of particles is the initial concept of the LGM, from the point of view of MD, the layer distribution appears as a result of calculations of the distribution functions of particles across the cross section of a slitlike pore (Gelb et al., 1999; Tovbin, 1997a; Berlin et al., 2002). It was shown that, in a narrow pore $6.5\sigma$ wide, a fluid formed a layered structure at $\rho_1 = 0.734$ ($\rho_1 = \theta/\mathrm{v}_0$). Six layers of approximately equal thickness were observed, and the density of these layers depended on the interaction energy between the fluid and pore walls (Berlin et al., 2002). Similar layer distributions were obtained in this work for all variants of the calculations in which the total adsorbate density and the interaction energy between the adsorbate and pore walls varied. This result allows the mean adsorbate densities within each layer to be related to the local degrees of layer fillings in the LGM. It follows that MD calculations substantiate the layer distribution of particles and the division of the volume of a pore into layers in the LGM.

To monitor the redistribution of particles in the LGM at the initial time, a "label" of a unit concentration was introduced in a particular layer. Further, we tracked its distribution between pore layers at various moments in time under the conditions of the equilibrium distribution of all system particles. This process of exchange of labeled particles between layers is described

by a discrete system of equations of the form

$$\frac{dP_g}{dt} = \sum_{f=g\pm1} \left(D^*_{fg}\, P_f - D^*_{gf}\, P_f\right), \qquad (13)$$

where $P_g$ is the concentration of labeled molecules in layer $g$ (here, $g, f \in$ H; that is, molecules cannot jump inside pore walls because of their impermeability). Dynamic system (13) was solved using the $P_g = 1$ initial condition for the layer into which the label was introduced and the $P_g = 0$ initial condition for the other layers.

Similarly, a pore was divided into layers of equal thickness in molecular dynamics simulations according to the calculated fluid density profile, and the $P_g(t)$ probabilities of particles occurring in layer $g$ at time $t$ were calculated.

### 3.2. *Comparison Between MD and LGM Results for Pure Fluid*

Calculations by both methods for a slitlike pore of width $H = 6.5\sigma$ were performed with changing temperature from $\tau = \varepsilon_{ArAr}/k_B = 0.6$ to 4.0. The lower temperature was close to the freezing point of the fluid, and the higher one lay in the region of high supercritical temperatures. We used a simple cubic lattice structure in LGM calculations; the number of the nearest neighbors was $z = 6$. This structure best corresponded to the critical parameters in the bulk phase (Hirschfelder et al., 1954; Barker et al., 1976; Batalin et al., 1980). Note that we used equal potential parameters in the LGM and MD calculations (no adjustment of the lattice parameter $\varepsilon_{\mathrm{ArAr}}$, was performed), although, according to (Tovbin et al., 1999a), energy $\varepsilon_{\mathrm{ArAr}}$ should be lower than the same value used in molecular dynamics.

The relative arrangement of the temperature dependences of the concentration profiles $\theta_f$ at various adsorbate - wall potential values obtained in the LGM and MD calculations is illustrated by Fig. 1. For instance, the MD calculations predict a weak temperature dependence for weak wall-adsorbate interactions (the first two families of curves corresponding to $\varepsilon_{\mathrm{wAr}}/\varepsilon_{\mathrm{ArAr}} =$ 0 and 1.81). The density of the surface layer is higher than that of the central layer for $\varepsilon_{\mathrm{wAr}} = 1.81$ because of attraction to the wall, whereas with $\varepsilon_{\mathrm{wAr}} = 0$, the density of the central layer is higher than that of the surface layer. In both cases, the density of the second layer is intermediate between $\theta_1$ and $\theta_3$ and shifted toward $\theta_3$. The general character of the arrangement of the $\theta_f(\tau)$ curves does not change from the molecular dynamics to lattice gas model calculations. The discrepancies are of 1–5% at high temperatures and increase as the temperature decreases. The most pronounced differences correspond to $\tau < 1.5$.

For walls with strong adsorbate attraction ($\varepsilon_{\mathrm{wAr}}/\varepsilon_{\mathrm{ArAr}} = 9.24$ and 16.7), the surface layer is virtually occupied, and the degree of filling of the third layer is substantially lower. This difference increases as temperature lowers. Qualitatively, both methods predict similar trends. At high temperatures, the differences are 1–10%, The differences increase to 15% as the temperature drops to $\tau \sim 1.5$. A further decrease in the temperature increases the differences for the second and third layers, whereas the differences for the first layer disappear. The nature of such behavior of the concentration profile is related to the condensation of molecules in different layers. Equations (4) and (5) do not describe these effects. Nevertheless, the LGM correctly predicts the behavior of the $\theta_f(\tau)$ curves in a wide temperature range.

Typical $P_g$(t) dependences obtained by both methods for $g =$ 1–6 and $\alpha = 0.3$ are shown in Fig. 2. The time dependences of the local carbon pore fillings with argon atoms shown in Fig. 2 refer to the case when the whole label is concentrated in the first monolayer at the initial time. Exchange between layers gradually increases the concentration of the label in layers $g =$ 2–6. Even at such a short distance as six monolayers, the delay of label front propagation manifests itself. This differentiates the discrete description of the label flow from a purely diffusion description (usually made using partial derivative equations). The curves describe the typical behavior of dynamic curves observed at different total pore fillings; the concentration profiles obtained by the two methods are in agreement with each other. The largest discrepancies (up to 30%) are those for the first, second, and sixth monolayers. The LGM and MD curves for layers 3–5 virtually coincide. At times longer than 75 ps, the dynamic curves reach their stationary values corresponding to equilibrium adsorbate distributions over the pore cross section.

The dynamic curves of interlayer label exchange at $\alpha = 0.34$ are shown in Fig. 3. Number $g$ corresponds to the layer number $g \leq 3$; the number of layers was reduced to simplify the drawings. The calculations refer to (*a*) $\varepsilon_{\mathrm{wAr}} = 5.16$ at $\tau = 1.0$ and (*b*) $\varepsilon_{\mathrm{wAr}} = 1$ and $\tau =$ 1.5. In the first case, atoms are held by the wall and, in the time interval up to 300 ps, the label virtually does

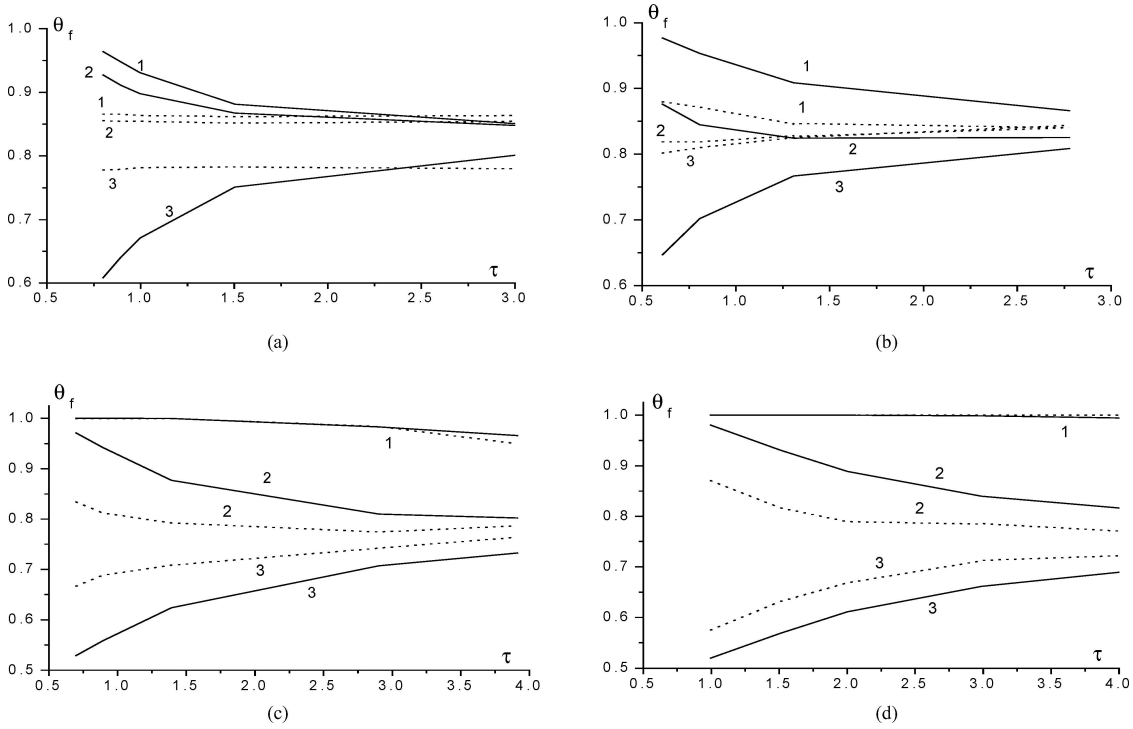


*Figure 1.* Temperature dependences of local fillings ($\theta_f$) in a slitlike pore with $H = 6.5\sigma$ at average density $\theta = 0.833$ calculated by MD (dots) and LGM (lines) simulations. Curve numbers are monolayer numbers. The wall-adsorbate interactions are $\varepsilon_{wAr}/\varepsilon_{ArAr} = 0$ (a), 1.81 (b), 9.24 (c), and 16.7 ( d).

not leave the first layer (the MD and the LGM calculations give coinciding $P_1$ values). If the label is placed into the second (Fig. 3(a)) or third layer we observe virtually no exchange of these layers with the first one,

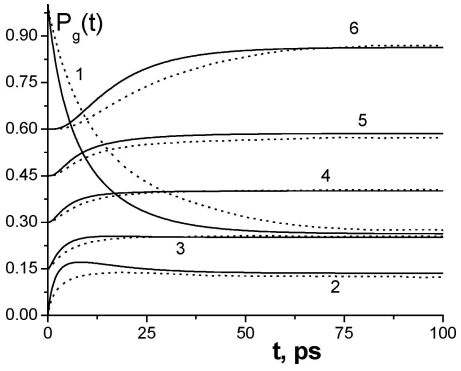


*Figure 2.* Dynamics of interlayer exchange of trace argon atoms between six layers ($i = 1$–$6$) in the carbon slitlike pore ($\varepsilon_{wAr}/\varepsilon_{ArAr} = 9.24$) at $\tau = 3.0$. The evolution of the degrees of filling layers $i = 1$–$6$ is described by LGM (lines) and MD (dots) methods. The curves for layers 3–6 are sequentially shifted upward along the axis of ordinates in order not to overcrowd the figure.

and exchange only occurs within the second and third layers. These curves asymptotically tend to the equilibrium $\theta_f$ values. The difference between the molecular dynamics and lattice gas model curves is caused by the difference in the $\theta_f$ values, whereas the extensions of dynamic curve transition regions obtained by the two methods are close to each other. The second group of curves corresponds to weak argon attraction by pore walls and $\tau = 1.5$. For these conditions, the curves virtually coincide over the whole time interval.

The temperature dependences of the mean self-diffusion coefficients along the pore axis obtained in molecular dynamics and lattice gas model calculations for different adsorbate — adsorbent interaction potentials are compared in Fig. 4. The curves for strongly attracting walls are fairly close to each other, but the curves for walls without the attraction potential branch are noticeably different. Curves 4–7 within the LGM were obtained with one parameter $a$ value. Generally, this parameter may depend on temperature and density (Tovbin et al., 1999a). Taking this dependence into account (curve 7) allowed us to obtain a virtually exact

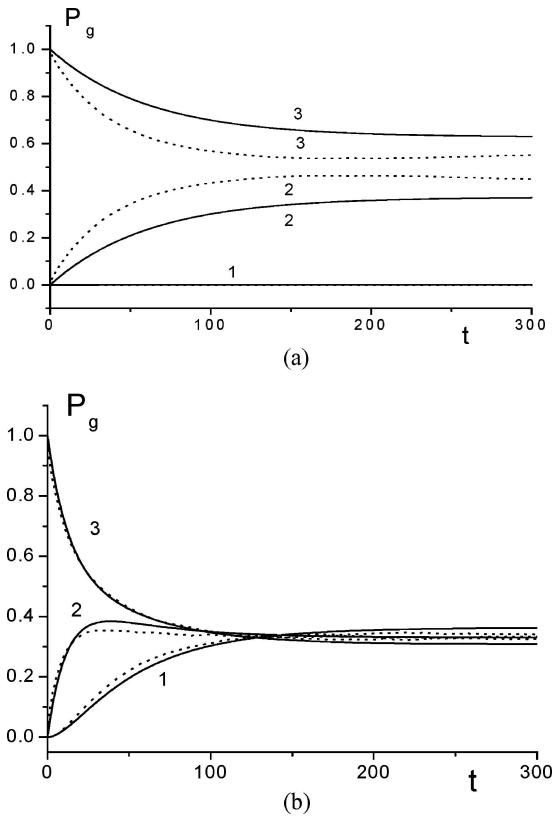


*Figure 3.* Dynamics of interlayer exchange of trace argon atoms in (*a*) the carbon slitlike pore ($\varepsilon_{wAr}/\varepsilon_{ArAr} = 9.24$) at $\tau = 1.0$, and (*b*) polymer matrix at $\tau = 1.5$ ($\varepsilon_{wAr}/\varepsilon_{ArAr} = 1.81$). At the initial time, the trace particles refer to the second layer for Fig. 3(a), and to third layer for Fig. 3(b). As below, the evolution of the total degrees of filling layers $f = 1$–$3$ is described by LGM (lines) and MD (dots) methods.

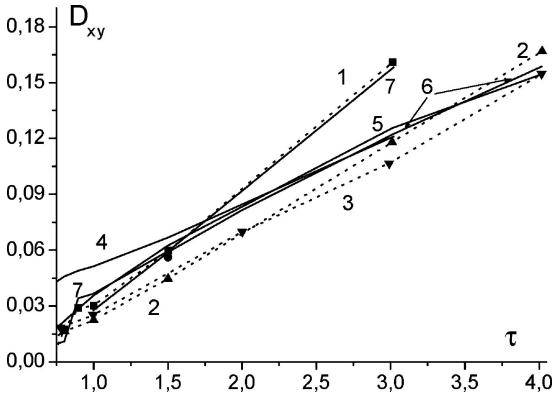


*Figure 4.* The temperature dependences of the self-diffusion coefficients of argon atoms in the slitlike pores at $\alpha = 0.34$ for $\varepsilon_{wAr}/\varepsilon_{ArAr}$ = 0 (1, 4, 7), 9.24 ( 2, 5) and 16.7 (3, 6). Dots and lines correspond to the MD (1–3) and LGM (4–7), respectively.

coincidence with the molecular dynamics data by increasing $a$ at high temperatures and decreasing it by the same value at low temperatures (the largest change in $\alpha$ at the extreme points of the $t$ interval did not exceed 50%).

### *3.3. Equilibrium Dependences of Binary Mixture Systems*

Our calculations deal with a one-phase state of the mixture. The temperature was fixed as $T/T_{crit} = 1.38$ for pure argon fluid in the slitlike pore of 10 monolayers width (for pure krypton fluid this ratio corresponds to 1.06). The equilibrium characteristics of the binary mixture are shown in Figs. 5–7. The structure $z$ of the fluid mixture was modeled by a lattice with twelve nearest neighbors. The local degrees of filling with argon and krypton atoms in different monolayers are shown in Fig. 5 for five vapor compositions at fixed overall densities of the mixture $\theta = \theta_1 + \theta_2 = 0.25$ (Fig. 5(a)) and 0.75 (Fig. 5(b)). The calculations were performed for the mole fractions of the second component $\gamma = P_2/P = 0$, 1/3, 1/2, 2/3, and 1.0 (where, $P = P_1 + P_2$, $P$ is the total vapor pressure). In Fig. 5, abscissa values are monolayer numbers. Because the walls of a slitlike pore are identical, the component distributions over the pore section (Figs. 5(a) and 5(b)) are symmetrical with respect to the pore center.

Figure 5 (a) corresponds to a comparatively low overall degree of filling ($\theta = 0.25$); both components are concentrated near the walls, and the central part of the pore is filled to a much lesser degree. Krypton atoms are attracted more strongly, and, in the absence of argon, their concentration in the surface layer is higher (curve 5(b)) than the concentration of pure argon (curve *1*a). The concentration of the first component near the walls decreases as the fraction of the second component $\gamma$ increases. The influence of the wall potential extends through three monolayers, its contribution to the fourth and fifth monolayer is small. All the curves have similar shapes with a concentration minimum in the center of the pore.

The distribution of components becomes more complex for substantial pore volume fillings ($\theta = 0.75$, Fig. 5(b)). For pure components, the density is as previously minimum in the center of the pore (curves 1a and 5b). The difference between the concentration in the center of the pore and the surface concentration is, however, much smaller. As previously, the potential of the wall influences three monolayers on each side of

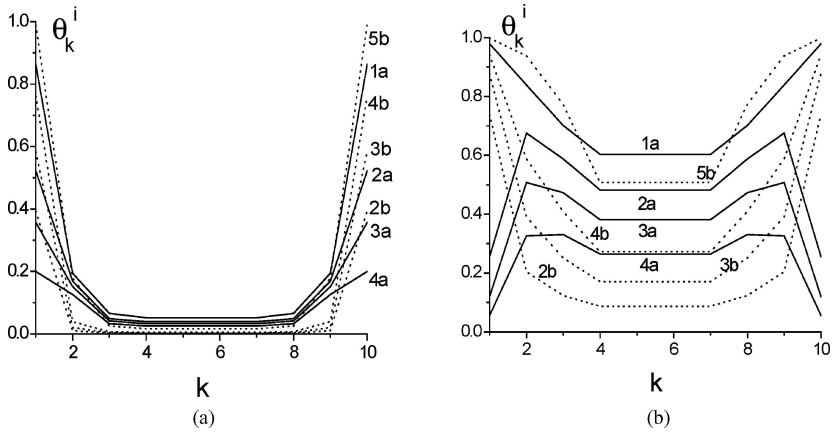


*Figure 5.* Component distributions of argon ($i = 1$) and krypton ($i = 2$) atoms over the pore section in a slitlike symmetrical graphite pore of width 10 monolayers ($k$ is the monolayer number, $1 \leq k \leq 10$) at $\theta = 0.25$ ( a) and 0.75 ( b) for five vapor compositions: $\gamma = P_2 / P = 0$ (*1*), 1/3 (*2*), 1/2 (*3*), 2/3 (*4*), and 1.0 (*5*), ($P = P_1 + P_2$). Curve numbers correspond to $\gamma$ values. Indices *a* (solid lines) and *b* (dashed lines) refer to argon and krypton, respectively.

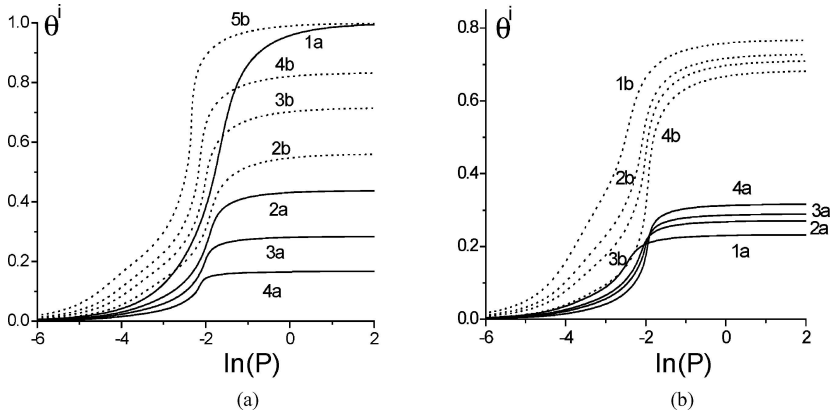


*Figure 6.* Average partial isotherms of binary mixtures in slitlike symmetrical graphite pores as functions of the total vapor pressure *P*. (a) Average partial isotherms $\theta_i(P)$ of argon and krypton in 10 monolayers pore width for five vapor mixture compositions $\gamma$ (as on Fig. 5). (b) Influence of the pore width on the average partial isotherms of argon (a) and krypton (b) for $\gamma = 0.5$: $H = 5$ (*1*), 8 (*2*), 11 (*3*), and 25 (*4*) monolayers.

the pore. The appearance of the krypton in mixtures results in its predominant accumulation near the pore walls. It displaces argon from the surface layer, and the distribution of argon over the pore section has maxima in the region of the second or third monolayer, whereas the concentration of krypton monotonically decreases from the walls to the pore center (as in Fig. 5(a)).

In Fig. 6, the logarithms of the total vapor pressure are plotted as abscissas. The mean partial isotherms at variable $\gamma$ values and pore width $H$ are shown in Figs. 6(a) and 6(b). In Fig. 7, the partial local fillings of the first and fourth monolayers are given for various second component interactions with the pore wall ${Q_1}^2$ and lateral interactions between second component particles.

The degree of filling of each monolayer increases as the total pressure grows (Fig. 6(a)). The surface monolayers are filled first, next go the second etc. (counting from the pore walls) monolayers. The stronger attraction of krypton shifts all partial isotherms to lower total pressures compared with the partial isotherms of argon. The influence of the width of a slitlike pore ($H$ = 5, 8, 11, and 25 monolayers) on the mean partial isotherms of mixture components is shown in Fig. 6(b),

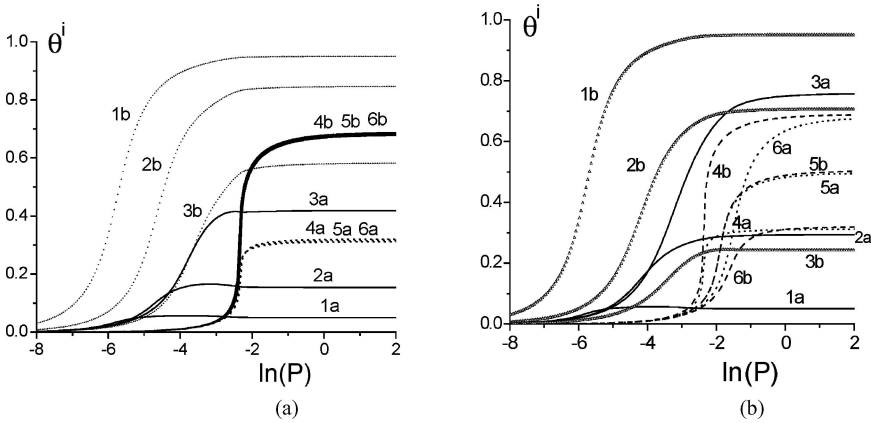


*Figure 7.* Partial local isotherms for the surface layer (1—3) and for the central region (4–6) (as above a corresponds to argon, and b corresponds to krypton); (*a*) Influence of the interaction energy between the second component and the pore wall: ${Q_1}^2/\varepsilon_{\mathrm{ArAr}} = 12.2$ (1, 4), 9.2 (2, 5), and 6.2 (3, 6); (b) Influence of the interparticle interaction energy on average partial local isotherms: $\varepsilon_{22}/\varepsilon_{\mathrm{ArAr}} = 1.37$ (1, 4), 1.0 (2, 5), and 0.63 (3, 6).

where partial fillings are plotted depending on the total vapor pressure $p$ for $\gamma = 0.5$. The smaller H, the more rapidly is the pore filled because of the influence of the attracting wall potential. A further increase in the pore width weakly influences the conditions of filling the central part of the pore, where the influence of the wall potential is zero. The degree of filling with krypton is always higher than that with argon.

The influence of the potential functions on the partial local isotherms is shown in Fig. 7. The local degrees of filling the surface and central monolayers are given; these results characterize the total range of changes in all local fillings at $\gamma = 0.5$. In Fig. 7(a), the depth of the potential well for the interaction between the second mixture component and the walls is varied at a constant $\varepsilon_{22}$ parameter corresponding to krypton (the first component is argon). A decrease in ${Q_1}^2$ decreases the degree of filling of the surface layer with the second component and increases the degree of filling with the first component, whereas the local partial isotherms for the central part of the pore remain virtually unchanged. The differences between the partial isotherms of the second component for the surface monolayer (2b and 3b) and similar isotherms of the first component *(2*a and 3b) evidence that intermolecular interactions play an important role in filling pores. The curves in Fig. 7(b) show this in more detail. In this figure, the depth of the potential well for the interaction between second component (krypton) atoms $\varepsilon_{22}$ is varied at $Q_1^2 = \mathrm{const}$ (the first component is argon). A decrease in $\varepsilon_{22}$ sharply decreases the degree of filling of the surface layer with the second component and increases the degree of filling with the first component. Simultaneously, the degree of filling of the central part of the pore with the second component and the fraction of the first component sharply decrease. This result shows that, while the wall potential influences near-surface layers, intermolecular interaction effects are noticeable over the whole pore volume.

### *3.4. Concentration Dependences of Self-Diffusion Coefficients*

All the concentration curves were normalized with respect to the corresponding self-diffusion coefficient of argon atoms in the gaseous phase (at $Q_1^1 = 0$ and $\theta = 0$). Concentration dependences of the self-diffusion coefficients for argon atoms, local and cross section average, in the carbon pore 10 monolayers wide are shown in Fig. 8. Here and below, $\alpha_{11} = E_{11}^{iv}/Q_1^i = 0.1$ is the height of the low activation barrier to surface jumps.

All local coefficients decrease as the degree of pore filling increases because of a decrease in the free pore volume. Motion of particles in the first (surface) layer changes most sharply (curve *1*). Filling this layer causes the self-diffusion coefficient to fall abruptly at $\theta < 0.2$, that is, when the monolayer is formed. A further increase in $D_{11}^*$ is caused by film compaction. Particles passage from the first to the second monolayer requires overcoming bond energy $Q_1$, and curve *2* for $D_{12}^*$ is therefore situated below all other curves. The $D_{21}^*$

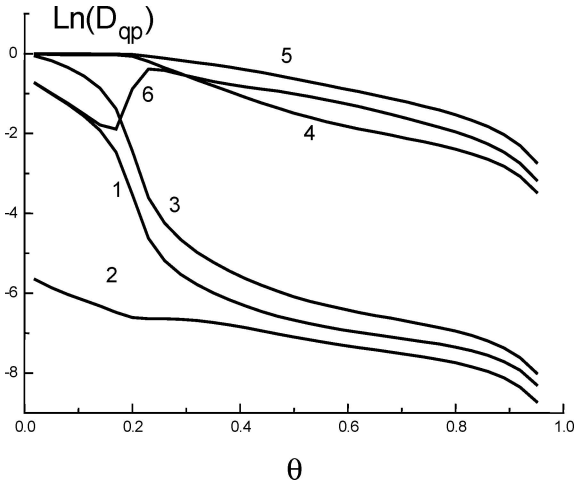


*Figure 8.* Concentration dependences of local self-diffusion coefficients for the argon-carbon system at $\alpha = 0.5$ and $\alpha_{11} = 0.1$. The curves correspond to the following pairs of neighboring cells in layers: $fg = 11$ (1), 12 (2), 21 (3), 22 (4) and 55 (5). Curve 6 corrsponds to the average $D^*$ value.

coefficient corresponds to the back transfer of particles from the second layer to the first; the shape of curve *3* for this coefficient, which decreases as a degree of filling of the first layer increases, reproduces that of curve *1*. Movement of particles in the second layer (curve *4*) at low filling occurs as in the center of the pore (curve *5*). The $D^*_{22}$ coefficient begins to decrease at $\theta > 0.2$, when the first monolayer is filled. The average diffusion coefficient $D^*$ has a non-monotonic $\theta$ dependence. This value is determined by the contributions of filling from all layers and therefore close to $D^*_{11}$ at low and to $D^*_{55}$ at high fillings. The ratio between $D^*(\theta = 0)$ and the $D^*$ value at the point of its maximum depends on the $E^{iv}_{11}$ activation energy of surface migration, and the lower $E^{iv}_{11}$, the higher $D^*(\theta = 0)$.

The concentration dependences of self-diffusion coefficients shown in Fig. 9 correspond to the molecular parameters $H = 10$, $\alpha = 0.5$, $\alpha_{11} = 0.1$ and $Q^1_1 = 9.24$ $\varepsilon_{\mathrm{ArAr}}$. All curves are normalized with respect to the self-diffusion coefficient of argon in the gas phase. The local self-diffusion coefficients of argon (solid lines) (a) and krypton (dashed lines) (b), which depend on the distance from the pore walls and the direction of migration, and the average partial self-diffusion coefficients are shown in Fig. 9. These concentration curves are similar to the ones for the pure fluid. The partial self-diffusion coefficients of both components decrease as the centers of various types get filled. First, the local coefficients for the surface monolayer and, last, those for the central region decrease as the pressure increases. The average self-diffusion coefficients vary non-monotonically. They have maxima in the region of surface monolayer filling, and when this layer is virtually filled, the filling of the second layer begins. In this situation, migration in the second monolayer occurs at a fairly high rate. As the volume of pores gets filled, the fraction of free sites lowers, and all self-diffusion coefficients decrease.

The average values for various mixture compositions are shown in Fig. 10. The initial argon and krypton self-diffusion coefficients remain unchanged as the

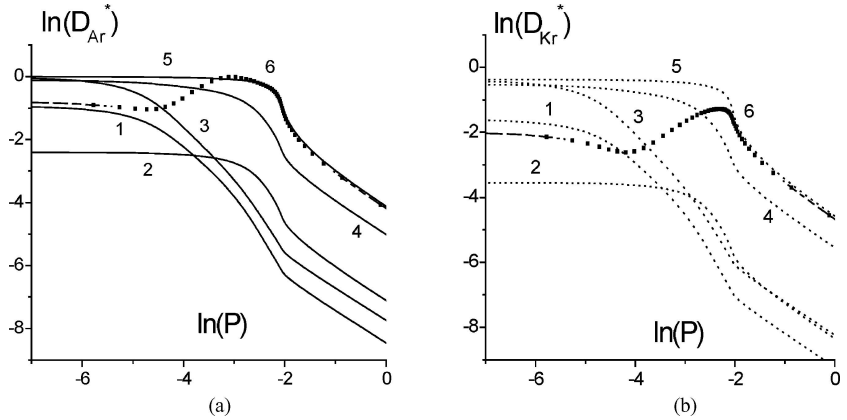


*Figure 9.* Concentration dependences of local partial self-diffusion coefficients $D^{*i}_{fg}$ for label (*a*) argon and (*b*) krypton atoms in the binary mixture at $\gamma = 0.5$ in a carbon slitlike pore at $H = 10$, $\alpha = 0.5$, $\alpha_{11} = 0.1$, and $Q_1{}^1 = 9.24\varepsilon_{\mathrm{ArAr}}$. The curves correspond to the following pairs of neighboring cells in layers $fg$ and the average $D^*{}_i$ value as on Fig. 8.

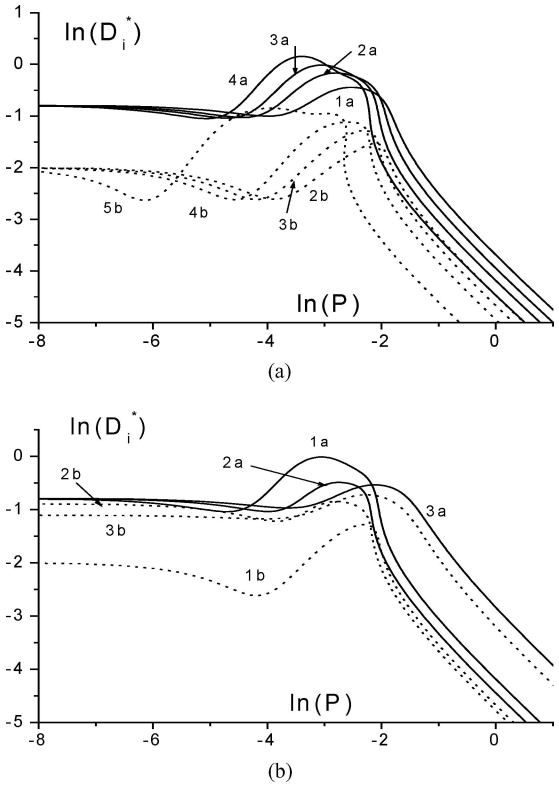


*Figure 10.* Concentration dependences of average self-diffusion coefficients $D^*_i$ in slitlike pores (calculation conditions as on Fig. 9). (*a*) Variation of the argon–krypton mixture composition: $\gamma = 0$ (1), 1/3 (2), 1/ 2 (3), 2/3 (4), and 1.0 (5). (*b*) Influence of the molecular parameters for the second component on $D^*_i$ values at $\gamma = 0.5$: for the argon–krypton mixture (*1*), and for mixtures with changed second component parameters (2, 3): (2) $Q_1^2 = 6.2\varepsilon_{\mathrm{ArAr}}$ and $\varepsilon_{22} = \varepsilon_{\mathrm{KrKr}}$; and (3) ${Q_1}^2 = 12.2\varepsilon_{\mathrm{ArAr}}$ and $\varepsilon_{22} = 0.46\varepsilon_{\mathrm{KrKr}}$.

composition of the mixture varies, because, at low pressures (fillings), the mobility of each component is independent of the presence of other particles. Argon and krypton have different masses and activation energies of surface migration. As previously, the average self-diffusion coefficients pass maxima as the pressure increases (Fig. 10(a)).

The influence of the molecular parameters of the adsorption system $Q_1^2$ and $\varepsilon_{22}$ is shown in Fig. 10(b) [the properties of the first component (argon) are fixed]. At the given $\gamma = 0.5$ value, the influence of the molecular properties of the second component on the mobility of argon becomes noticeable at fairly high degrees of filling. A decrease in the interaction energy with the surface (curve 2b) substantially increases the self-diffusion coefficient of the second component and influences the mobility of argon, though to a lesser degree. A decrease in intermolecular interactions for the second component at strong attraction by the walls makes the concentration dependences for the two components closer to each other. The data obtained are evidence of a strong influence of the molecular properties of mixture components on changes in the self-diffusion coefficients as the total density of a mixture of fluids varies.

## 4. Conclusions

The results obtained in this work show that the simplest variant of the LGM gives satisfactory agreement with the MD data at supercritical temperatures for both the concentration profiles of adsorbate distributions in a narrow slitlike pore and the average self-diffusion coefficients of a label along the pore axis. This allows the LGM to be used to substantially speed up calculations of molecular distributions. It appears that the most natural variant of using LGM is its joint use with the MD method, when calculations for several limiting situations are performed by MD, and LGM simulation are used to perform mass calculations in wide temperature and concentration ranges (that is, the LGM is a convenient interpolation method). In addition, the LGM allows us to go beyond the limitations imposed by large time expenditures and analyze dynamic processes over long periods.

According to the LGM equations, the self-diffusion coefficients depend on the lattice parameters, which are directly related to atom–atom potentials between molecules and between molecules and pore walls. The activation energies of molecular displacements $E^{iv}_{fg}$ depend on the energy states of molecules in various cells, which are expressed in terms of the interaction potential between a particle and pore walls. Our calculations show that the dynamic characteristics of an adsorbate strongly depend on the anisotropic distribution of molecules across slitlike pores. The self-diffusion coefficients change most substantially near pore walls. These values in the center of a pore depend on the contribution of the wall potential and the total concentration of the mixed adsorbate. An analysis of experimental data should be performed taking into account the fairly strong concentration dependence of the partial dynamic characteristics of mixtures of adsorbates in narrow pores caused by both the influence of the potential of pore walls and intermolecular interactions.

## Acknowledgment

This work was financially supported by the Russian Foundation for Basic Research (project no. 03-03-32072).

## References

Akhmatskaya, E., B.D. Todd, P.J. Davis, D.J. Evans, K.E. Gubbins, and L.A.Pozhar, *J. Chem. Phys*., **106**, 4684–4695 (1997).

Barker, J.A. and D. Henderson, *Rev. Mod. Phys.*, **48**, 587–671 (1976).

Batalin, O.Yu., Yu.K. Tovbin and V.K. Fedyanin, *Russ. J. Phys. Chem*., **53**, 3020–3025 (1980).

Berlin, A.A., M.A. Mazo, N.K. Balabaev, and Yu.K. Tovbin, "Single-Component and Two-Component Mixtures in Slit-Like Pores: Molecular Dynamics Simulation", K. Kaneko, H. Kanoh and Y. Hanzawa (Eds.), *Fundamentals of Adsorption* - 7, IK International, Ltd., Chiba-City, 2002 pp. 402–409.

Dubinin M.M. and V.V. Serpinskii (Eds.), Adsorption *in Micropores*, Nauka, Moscow, pp. 114 – 170 1983.

Gelb, L.D., K.E. Gubbins, R. Radhakrishnan, and M. Sliwinska-Bartkowiak, *Rep. Prog. Phys*., **62**, 1573–1659 (1999).

Glasstone, S., K.J. Laidler, and H. Eyring, *The Theory of Rate Processes.*, McGraw-Hill, New York, 1941.

Hill, T.L., *Statistical Mechanics. Principles and Selected Applications*. McGraw-Hill Book Comp. Inc., New York, 1956.

Hirschfelder, J.O., C.F. Curtiss and R.B. Bird, *Molecular Theory of Gases and Liquids.*, Wiley, New York, 1954.

Karger, J., *Adsorption*, **9**, 29–35 (2003)

Kheifets, L.I. and A.V. Neimark, *Multiphase Processes in Porous Media*, Khimiya, Moscow, 1982.

MacElroy J.M.D., *J. Chem. Phys*., **10**1, 5274–5284 (1994).

Mason, E.A. and A.P. Malinauskas, *Gas Transport in Porous Media: The Dusty-Gas Model*, Elsevier, Amsterdam, 1983.

Mazo, M.A., A.B. Rabinovich, and Yu.K. Tovbin, *Russ. J. Phys. Chem.*, **77**, 1848–1854 (2003).

Prigogine, I., *The Molecular Theory of Solutions*, North-Holland, Amsterdam, 1957.

Ruthven, D.M., *Principles of Adsorption and Adsorption Processes.* Wiley, New York, 1984.

Satterfield C.N., *Mass Transfer in Heterogeneous Catalysis*, Reinhold, New York, 1970.

Smirnova, N.A., *Molecular Theory of Solutions*, Khimiya, Leningrad, 1987.

Sokolowski, S. and J. Fischer, *Molecular Phys*., **71**, 393–412 (1990).

Steele, W.A., *The Interactions of Gases with Solid Surfaces* Pergamon, New York, 1974.

Timofeev, D. P. *Kinetics of Adsorption.*, Nauka, Moscow, 1962.

Todd, B.D. and D.J. Evans, *J. Chem. Phys*., **10**3, 9804–9809 (1995).

Tovbin, Yu.K., *Dokl. Akad. Nauk SSSR*, **27**7, 917–921 (1984).

Tovbin, Yu.K., *Doklady Akad. Nauk. SSSR*, **312**, 1423–1427 (1990a).

Tovbin, Yu.K., *Progress in Surface Sci*., **34**, 1–236 (1990b).

Tovbin, Yu.K., *Theory of Physical Chemistry Processes at a Gas–Solid Interface*, CRC Press, Boca Raton, Florida, 1991.

Tovbin, Yu.K. and E.V.Votyakov, *Langmuir*, **9**, 2652–2660 (1993).

Tovbin, Yu.K., "Application of lattice-gas model to describe mixed-gas adsorption equilibria", in W. Rudzinski, W.A. Steele, and G. Zgrablich (Eds.),*Dynamics of Gas Adsorption on Heterogeneous Solid Surfaces*, Elsevier, Amsterdam, pp. 105–152 1996.

Tovbin, Yu.K., "Sorption in porous systems", in "*Molecular Dynamics Method in Physical Chemistry*", Nauka, Moscow, pp. 128–178 1997a.

Tovbin, Yu.K., *Russ. Chem. Bull.*, **46**, 458–463 (1997b).

Tovbin, Yu.K., *Chem. Phys. Reports*, **17**, 1209-1222 (1998a).

Tovbin, Yu.K. and E.V. Votyakov, *Russ. J. Phys. Chem.*, **72**, 1885–1890 (1998b).

Tovbin, Yu.K., M.M. Senyavin, and L.K. Zhidkova, *Russ. J. Phys. Chem.*, **73**, 245–253 (1999a).

Tovbin, Yu.K., *Russ. Chem. Bull.*, **48**, 1467–1478 (1999b).

Tovbin, Yu.K., V.N. Komarov, and N.F. Vasyutkin, *Russ. J. Phys. Chem.*, **73**, 500–506 (1999c).

Tovbin, Yu.K. and N.F. Vasyutkin, *Russ. Chem. Bull.*, **50**, 1496–1501(2001a).

Tovbin, Yu.K. and E.V. Votyakov, *Russ. Chem. Bull.*, **50**, 48–56 (2001b).

Tovbin, Yu.K., L.K. Zhidkova, and V.K. Komarov, *Russ. Chem. Bull.*, **50**, 752–758 (2001c).

Tovbin, Yu.K., "Volume filling of pores and a classification of porous systems" in *Proceedings of Conference Dedicated to the 100th Anniversary of M. M. Dubinin*, Inst. Fiz. Khim. Russ. Akad. Nauk, Moscow, pp. 27–32 2001d.

Tovbin, Yu.K. and N.F. Vasyutkin, *Russ. J. Phys. Chem.*, **76**, 319–324 (2002a).

Tovbin, Yu.K., A. B. Rabinovich, and E.V. Votyakov, *Russ. Chem. Bull.*, **51**, 1531–1538 (2002b).

Tovbin, Yu.K. and V.N. Komarov, *Russ. Chem. Bull.*, **51**, 1871–1880 (2002c).

Tovbin, Yu.K., E.E. Gvozdeva, and D.V. Yeremich, *Russ. J. Phys. Chem*., **77**, 878–883 (2003a).

Tovbin, Yu.K., *Russ. J. Phys. Chem.*, **77**, 2134–2138 (2003b).

Tovbin, Yu.K., A.B. Rabinovich, and D.V. Yeremich, *Russ. J. Phys. Chem.*, **78**, 425–432 (2004).

Vartapetyan, R.Sh., A.M. Voloshchuk and I. Kerger, "Translational mobility of molecules adsorbed in carbon adsorbents", N.S. Polyakov (Ed.), in *Proceedings of the VII International Conference "Theory and Practice of Adsorption Processes"*, pp. 63–68, Inst. Fiz. Khim. Ross. Akad. Nauk, Moscow, 1997.

Vishnyakov, A., E.M. Piotrovskaya, E.N. Brodskaya, et al., *Russ. J. Phys. Chem.*, **74**, 221–226 (2000).

Votyakov, E.V., Yu. K. Tovbin, J. M. D. MacElroy, and A. Roche, *Langmuir*, **1**5, 5713–5721 (1999).